Cysteine residues in the cytoplasmic carboxy terminus of connexins dictate gap junction plaque stability

Randy F. Stout, Jr.[a,b,*], and **David C. Spray**[b]
[a]Department of Biomedical Sciences, New York Institute of Technology College of Osteopathic Medicine, Old Westbury, NY 11568-8000; [b]Dominick P. Purpura Department of Neuroscience, Albert Einstein College of Medicine, Bronx, NY 10461

ABSTRACT Gap junctions are cellular contact sites composed of clustered connexin transmembrane proteins that act in dual capacities as channels for direct intercellular exchange of small molecules and as structural adhesion complexes known as gap junction nexuses. Depending on the connexin isoform, the cluster of channels (the gap junction plaque) can be stably or fluidly arranged. Here we used confocal microscopy and mutational analysis to identify the residues within the connexin proteins that determine gap junction plaque stability. We found that stability is altered by changing redox balance using a reducing agent—indicating gap junction nexus stability is modifiable. Stability of the arrangement of connexins is thought to regulate intercellular communication by establishing an ordered supramolecular platform. By identifying the residues that establish plaque stability, these studies lay the groundwork for exploration of mechanisms by which gap junction nexus stability modulates intercellular communication.

INTRODUCTION

Gap junction (GJ) channels are axially aligned hexamers of connexin proteins that interconnect the cytoplasm of adjacent cells. The multiple connexin isoforms (21 in humans) are expressed in specific and overlapping cell populations. GJ channels are clustered into discoid GJ plaques, which together with specific protein binding partners for each connexin form the supramolecular gap junction nexus (Duffy et al., 2002).

Although GJ plaques have generally been regarded as stable and homogeneous two-dimensional protein arrays, recent studies have revealed that the arrangement of certain types of GJ channels within the plaque is heterogeneous and depends on posttranslational modifications (Cone et al., 2014). For example, connexin 43 (Cx43) GJs are formed by accretion of newly synthesized channels at the periphery of the plaque, whereas older protein is retrieved from the plaque interior (Gaietta et al., 2002; Lauf et al., 2002; Falk et al., 2009). In addition, Cx43 that is phosphorylated on specific amino acid residues in its carboxy terminus (CT) has been shown to be localized to subdomains within Cx43 GJ plaques (Solan and Lampe, 2014). The arrangement of GJ channels within the plaque structure is expected to influence both junctional and nonchannel functions of GJs (Falk et al., 2009; Wayakanon et al., 2012; Bejarano et al., 2014; Pidoux et al., 2014; Solan and Lampe, 2014; Ambrosi et al., 2016; Dukic et al., 2017; Waxse et al., 2017).

A stable arrangement of Cx43 is a prerequisite for the ordered arrangement of channels within the plaque, and such stability has been demonstrated for certain connexins by photobleaching, photoconversion, and pulse-chase labelling strategies (Lauf et al., 2002; Sosinsky et al., 2003; Baker et al., 2010). We showed previously that Cx43 forms GJ plaques with substantially higher stability than GJs

made up of connexin 26 (Cx26) and connexin 30 (Cx30) (Stout *et al.*, 2015). Moreover, through mutagenesis to remove most of the CT (truncation at amino acid 258), we found that the CT of Cx43 is required for GJ plaque stability (Stout *et al.*, 2015). Interestingly, mice carrying this truncated Cx43 sequence have many defects in development and in mature function of several tissues (Maass *et al.*, 2004, 2007; Cina *et al.*, 2009; Maass *et al.*, 2009; Kozoriz *et al.*, 2010). Human mutations producing truncation of Cx43 at or before cysteine 260 have been identified in cases of the disease occulo-dentodigital dysplasia (ODDD) (Pizzuti *et al.*, 2004; Gong *et al.*, 2006). These frameshift mutations cause nonsense run-on sequences before reaching a stop codon, and it is unknown which of the myriad symptoms are caused by lack of gap junction communication or the elimination of the Cx43 CT, as recently reviewed (Kelly *et al.*, 2015). However, because truncation of Cx43 at amino acid 258 also removes most sites of posttranslational modification and protein-protein interaction, the mechanism by which the Cx43 CT anchors the position of GJ channels within the plaque has not been identified. Here we report results of studies in which site directed mutagenesis was used to identify the specific residues that provide an anchoring domain in connexins 32 and 43 to stabilize the position of the channels within the gap junction plaque structure. Consistent with the finding that cytoplasmic cysteine residues are required for stability, treatment with a reducing agent increases mobility of gap junction channels within the gap junction nexus.

RESULTS AND DISCUSSION

To identify the amino acid residues within the Cx43 CT required for stable GJ plaques, we performed serial truncation experiments using super folder GFP-tagged Cx43 (sfGFP-Cx43) with stop codons inserted at locations at and distal to amino acid 258 in the CT (Supplemental Figure S1) and expressed the tagged Cx43 in two cell lines. Fluorescence recovery after photobleaching (FRAP) was used to test the stability of the arrangement of GJ channels within the GJ plaque structure. This use of FRAP to test the stability of the arrangement of channels within GJ plaques is substantially different from the common use of FRAP and also should not be confused with FRAP used to measure strength of GJ channel-mediated coupling, as previously described (Stout *et al.*, 2015; Stout and Spray, 2016). Applying FRAP methodology to Cx43 serially truncated at its CT, we identified amino acids between 258 and 262 as sufficient for GJ stability (Figure 1, A–C). Addition of an amino acid sequence overlapping this region of the Cx43 CT *stabilized* Cx26 GJs that are normally *fluidly* arranged structures (a chimera of Cx26 and Cx43 CT amino acids 241–272, Cx26CT43; Figure 1, D–F). Sectional deletion experiments revealed that deletion of the Cx43 CT segment 241–260 did not alter stability of Cx43 within the plaque (Supplemental Figure S4F). This indicates that other residues between amino acids 261 and the CT (terminal amino acid 382) can act redundantly to stabilize Cx43 GJ plaques.

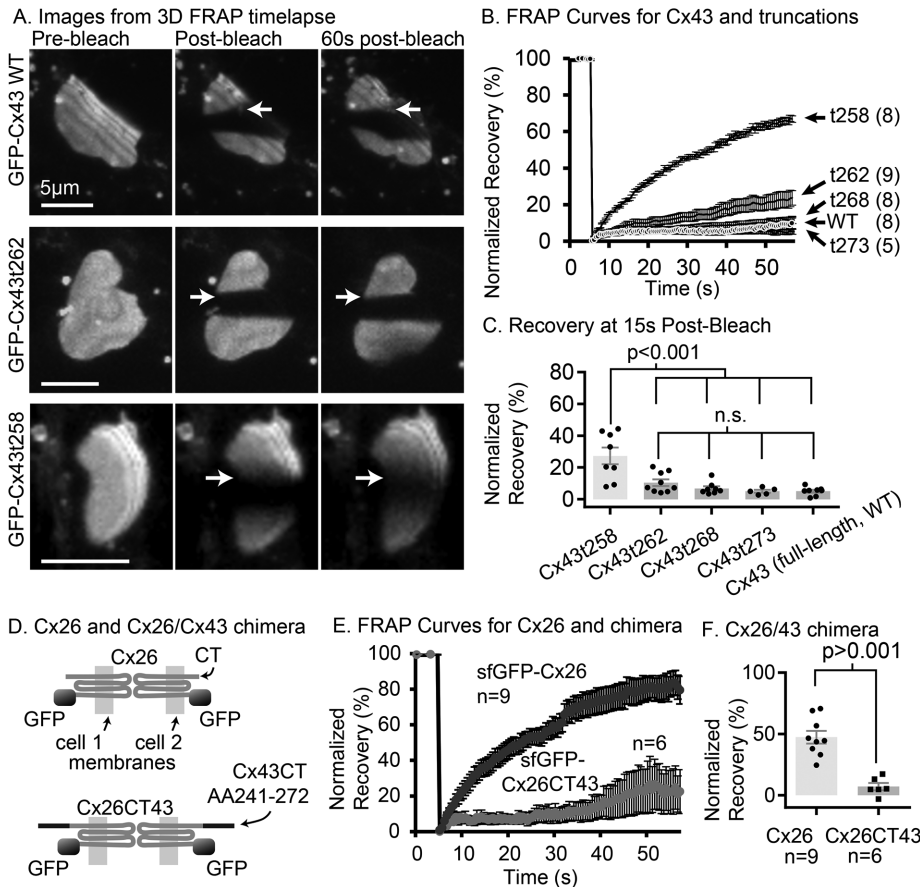Considering these results in conjunction with the sequences of the CT of connexins

FIGURE 1: The Cx43 cytoplasmic CT is necessary and sufficient to stabilize the arrangement of channels within the GJ plaque. (A) Volume reconstruction images from selected time points (as indicated above each column of images) from a three-dimensional time-lapse FRAP experiment with full-length Cx43 (top row), Cx43t262 (middle row, truncated at amino acid 262), and Cx43t258 (bottom row, truncated at amino acid 258) in HeLa cells (all constructs tagged with sfGFP on the amino terminus of the Cx43). Arrows point to the border between bleached and unbleached regions of the GJ plaque where recovery is most evident in the form of a *blurred* bleach-border in the case of Cx43t258 (lowest row of images) or, in the cases of Cx43 wt and Cx43t262, a lack of recovery evidenced by a *sharp* bleach-border after 60 s (top two rows, right column of three-dimensional image reconstructions). (B) Normalized, scaled recovery curves for Cx43 truncation mutants in HeLa cells, data from single-plane FRAP (two-dimensional time-lapse FRAP) with image interval of 0.5 s. (C) Percentage recovery at 15 s postbleach in HeLa cells (two-dimensional time-lapse FRAP) is significantly higher for sfGFP-Cx43t258 than for sfGFP-Cx43t262, sfGFP-Cx43t268, Cx43t273 and full-length Cx43 (sfGFP-Cx43-WT). Number of GJs tested is same as listed in B. Groups were compared by two-way analysis of variance followed by Tukey's multiple comparisons. (D) Cartoon showing that chimeric connexin Cx26CT43 has an amino terminal sfGFP tag, and the 30 amino acids from Cx43 (residues 241–272) containing the anchoring domain of Cx43 appended to the CT of Cx26. The membranes of the cells in which the connexins are embedded are indicated with light gray shading. (E) Recovery curves for sfGFP-Cx26, and sfGFP-Cx26CT43 in HeLa cells. (F) Percentage recovery at 15 s for wild-type Cx26 is significantly higher than sfGFP-Cx26CT43 by two-tailed Student's unpaired *t* test. A portion of the original image data for msfGFP-Cx43, and sfGFP-Cx43t258 was sourced from the data used for the Stout *et al.* (2015) study and reanalyzed with additional new data for those groups. Error bars in all histograms and graphs are SEM.
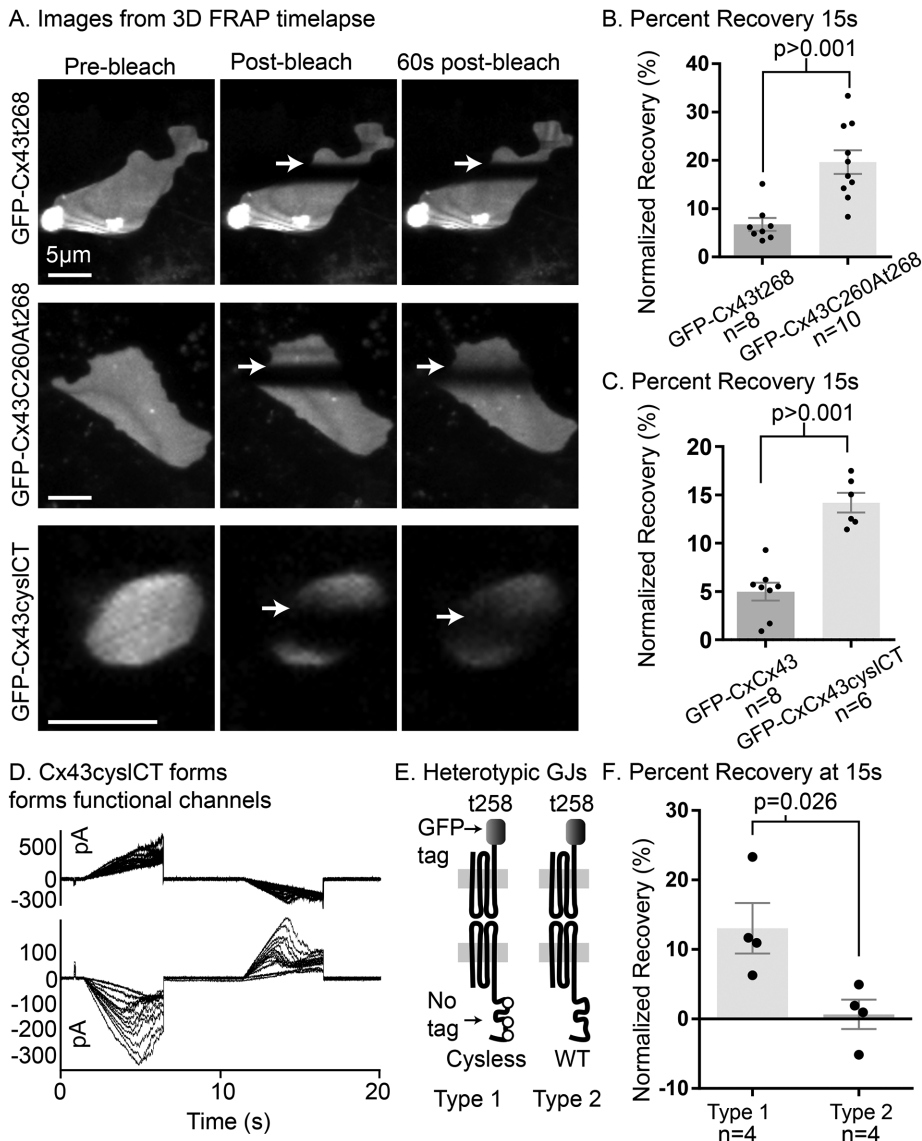
A. Images from 3D FRAP timelapse

B. Percent Recovery 15s

C. Percent Recovery 15s

D. Cx43cyslCT forms functional channels

E. Heterotypic GJs

F. Percent Recovery at 15s

FIGURE 2: Cysteine residues within the CT of Cx43 stabilize GJ plaques. (A) Volume reconstruction images from selected time points (indicated above columns) from a three-dimensional time-lapse FRAP experiment with full-length Cx43t268 (top row), Cx43C260A,t268 (middle row), and Cx43cyslCT (bottom row) in HeLa cells (all constructs tagged with sfGFP on the Cx43 amino-terminus). The location of the border of the bleached region of the plaques is indicated by arrows. Similar results were obtained in Neuro2A (N2A) cells as shown in Supplemental Video S1. (B) FRAP recovery for sfGFP-Cx43t268 and sfGFP-Cx43C260A,t268 in two-dimensional time-lapse experiments in HeLa cells 15 s after photobleaching. (C) Recovery at 15 s for wild-type Cx43 and Cx43cyslCT (with all cysteine residues in the CT mutated to alanine) using two-dimensional time-lapse FRAP in HeLa cells. (D) Untagged Cx43cyslCT overexpression produces functional GJ channels as shown by dual whole-cell voltage clamp with voltage ramps leading to GJ current flow from the upper cell to the lower cell in N2A cells. Voltage dependence characteristic for Cx43 is evidenced by the decreased junctional current at higher junctional voltages. Multiple superimposed sweeps were obtained during exposure to 2 mM heptanol, resulting in progressively decreasing junctional currents. (E) Cartoon illustration of the two types of heterotypically tagged GJ channels tested in F. (F) Percentage FRAP at 15 s for the types of Cx43t258-msfGFP and untagged Cx43 versus untagged Cx43cyslCT illustrated in E. Groups compared by Student's *t* test (two-tailed). A portion of the original image data for msfGFP-Cx43 and a portion of "Type 2 heterotypic GJs" in F were sourced from data used for the Stout *et al.* (2015) study and reanalyzed for this study.

residues within its CT. We found that a mutant form of Cx43 truncated at amino acid 268 (Cx43t268 which forms stably arranged gap junctions; Figure 1, B and C) but with an additional mutation of cysteine 260 to alanine (Cx43t268,C260A) is more mobile within GJ plaques than Cx43t268 with cysteine 260 intact (Figure 2, A and B). To test whether cysteine 260 and the other two cytoplasmic cysteine residues in the Cx43 CT act as the residues that anchor Cx43, we generated a full-length mutant form of Cx43 with all three cysteine residues in the CT mutated to alanine (Cx43C260,271,289A; referred to here as Cx43cyslCT). This construct formed fluidly arranged GJ plaques (Figure 2 and Supplemental Video S1). We found that varying bleach-laser intensity and bleaching time by several fold did not affect mobility of wild-type Cx43 (Supplemental Figure S3) or Cx43cyslCT (data not shown), ruling out photobleach-induced heating/oxidation of the Cx43 CT as the cause of GJ plaque stability established by the CT cysteine residues. Also, we note that in Supplemental Video S1, the morphological changes in the sfGFP-Cx43 (WT) are slower compared with the rapid morphology changes that can be seen for the sfGFP-Cx43cyslCT gap junction, even in areas of the plaque distal to the bleach region. These results indicate that photobleaching is not the cause of stability in gap junctions made up of wild-type Cx43. The stable plaque (sfGFP-Cx43 WT) does undergo some movement and shape change, however. This malleability (shown previously by others [Lauf *et al.*, 2002]) of stably arranged gap junctions implies that weak but highly abundant and frequent interactions between neighboring gap junctions stabilize the gap junction nexus structure. To monitor the impact of the untagged connexin on the mobility of the normally highly mobile Cx43t258-msfGFP, we used a strategy similar to one described previously in which a connexin truncation mutant (Cx43t258-msf-GFP, which was shown to be very fluid in GJ plaques [Stout *et al.*, 2015]) was expressed in one set of cells and an untagged connexin was expressed in another set. The two groups of cells are replated together (posttransfection) to generate heterotypic GJs (see Supplemental Figure S2). These studies revealed that untagged wild-type Cx43 effectively immobilized Cx43t258-msfGFP, whereas untagged Cx43cyslCT did not inhibit Cx43t258-msfGFP mobility (Figure 2, D–F, and Supplemental Figure

that form highly fluid GJ plaque structures (Cx26, Cx30 [Stout *et al.*, 2015], and Cx36 [Wang *et al.*, 2015]), we noticed that Cx43 differs from each of these connexins by having cytoplasmic cysteine

S4B), indicating that untagged Cx43cyslCT forms fluidly arranged GJ channels. We note that unlike the forms of Cx43 with an amino-terminal fluorescent protein tag used elsewhere in this study, the

channels examined for Figure 2E and Supplemental Figure S4B are functional since the apposing side of the gap junction plaques is made up of Cx43t258 with a carboxy-terminal tag (Cx43t258-msfGFP, shown to form very fluid GJ plaques [Stout *et al.*, 2015]). We suggest that sfGFP-Cx43cyslCT and variations of this construct will be useful for testing the effect of connexin mobility on the mobility of other GJ nexus components (allowing live visualization of plaque location) while the untagged form of Cx43cyslCT will be more useful for testing effects of GJ plaque arrangement stability on intercellular signaling.

Cx32 has two cysteine residues near the end of the cytoplasmic CT (C280, C283). We found that wild-type Cx32 forms stably arranged GJ plaques, whereas Cx32 with both cysteine residues in the CT mutated to alanine (Cx32cyslCT) formed highly fluid GJ plaques (Figure 3). Cx30 forms very fluidly arranged gap junctions (Stout *et al.*, 2015). Cx30 connexons can dock with Cx32 connexons to form heterotypic gap junction plaques and these structures have been observed through immunogold electron microscopy to connect astrocytes (Cx30) with oligodendrocytes (Cx32) (Rash *et al.*, 2001; Orthmann-Murphy *et al.*, 2007). We generated EBFP2-Cx30::sfGFP-Cx32 heterotypic gap junctions by transfecting separate populations of Neuro2A cells and then replating them together allowing heterotypic gap junction plaque formation. We performed FRAP experiments and measured recovery in the blue channel and found that EBFP2-Cx30 docked to wild-type Cx32 formed more stably arranged gap junction plaques than EBFP2-Cx30 docked to Cx32cyslCT (Figure 3C). This indicates that cysteine residues in the cytoplasmic portion of Cx32 expressed in one cell can dictate the mobility of a normally fluidly arranged connexin (Cx30) at a heterotypic gap junction plaque.
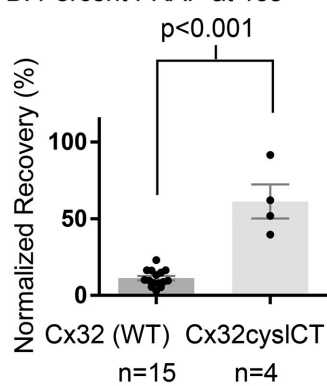
The additional cysteine residues present in the extracellular loops are defining features of connexins and have been long known to be critical for GJ channel formation and docking (Dahl *et al.*, 1992; Foote *et al.*, 1998) and to regulate unpaired hemichannel function (Retamal *et al.*, 2007). However, the cysteines we found to be critical for GJ plaque organization stability are localized to the cytoplasm and therefore tested for an effect of the cell permeable reducing agent dithiothreitrol (DTT; 10 mM for ≥6 h). We observed a significant decrease in stability when cells expressing the normally stable gap junction proteins Cx43 and Cx32 were exposed to these high amounts of DTT as shown in Figure 4. This implicates one of the many types of redox-dependent posttranslational modifications that can occur on cytoplasmic-localized cysteine residues. However, we did not detect an effect on stability for inhibitors of some modifications known to occur on cytoplasmic cysteine residues using the FRAP technique (Supplemental Figure S4G). We also note that there was a trend but no significant effect of DTT treatment in N2A cells expressing sfGFP-Cx43 (Supplemental Figure S4D), perhaps due to increased sensitivity of N2A cells to long-term treatment with high concentrations of DTT.

Cx43CyslessCT with alanine substitution retains channel function (Figure 2D). This is the first report showing that stability of the gap junction nexus can be altered through mutation without removing binding domains from the Cx43 CT and will allow testing for tissue level effects of nexus stability in vivo with particular attention to tissues in which connexin subdomains have functional significance such as neuro-gliovascular system, cardiovascular system, bone and cartilage development, tumor growth/metastasis, and skin-wound healing. The CT of Cx43 or Cx32 has been shown to be important in these tissues (Gellhaus *et al.*, 2004; Gago-Fuentes *et al.*, 2016; Hammond *et al.*, 2016; Katoch *et al.*, 2015). The cysteine residues of the CT of Cx43 (and some residues on either side of the cysteines) are conserved among rat and human sequences. We used the sequences for rat Cx43 (and Cx26) and human Cx32 in this study to show that this phenomenon is generalizable across connexin types and species. The GJ plaques we examined are very large but GJs within the range we tested in vitro have been found in vivo (Meyer *et al.*, 1981; Page *et al.*, 1983). We found that GJ plaque stability characteristics were consistent across the entire area of the GJ plaques: Wild-type Cx43 and C32 GJ plaques are stably arranged from center to edge (as seen in Figures 1–3, top rows of images). Since GJ plaque stability is modifiable and is only present in some connexins (Cx43 and Cx32) but not others (Cx26, Cx30, and Cx36) that are coexpressed in some tissues, we expect in vivo GJ plaque stability to vary according to tissue type and physiological condition. The stability characteristics of GJs in vivo will be an important area

A. Images from 3D FRAP timelapse
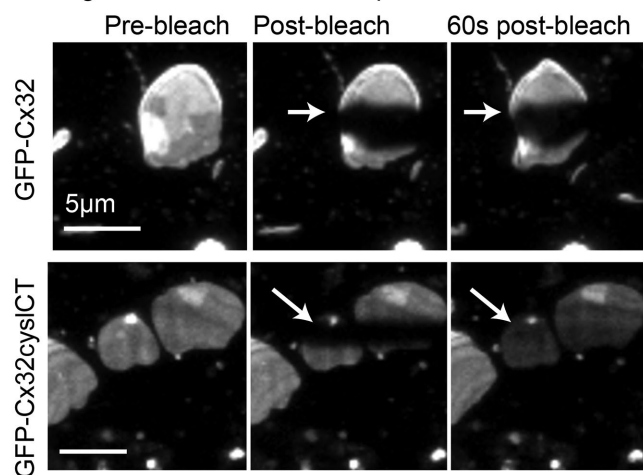
B. Percent FRAP at 15s   C. Cx30::Cx32 Heterotypic GJ plaques 15s N2A
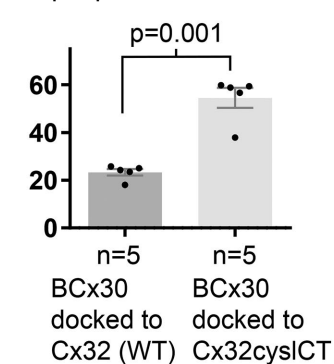

FIGURE 3: Cysteine residues in the CT of Cx32 restrict its mobility. (A) Three-dimensional time-lapse FRAP images of GFP tagged Cx32 and Cx32cyslCT in HeLa cells. The location of the border of the bleached region of the plaques is indicated by arrows; this border is not visible in the image of the msfGFP-Cx32cyslCT plaques 60 s postbleach because the unbleached protein has moved into the bleached region. (B) Percentage recovery of normalized fluorescence into the bleach region at 15 s for Cx32 and Cx32cyslessCT in HeLa cells using two-dimensional time-lapse FRAP. (C) The mobility of EBFP2-Cx30 (BCx30) is significantly reduced when it forms heterotypic GJ plaques with Cx32 compared with when it forms heterotypic gap junction plaques with Cx32cyslCT, as indicated by reduced recovery at 15 s for EBFP2-Cx30 at heterotypic plaques. N2A cells were used for experiments for C. Groups compared by Student's *t* test (two-tailed).

A. 3D FRAP timelapse of Cx43 with/without DTT
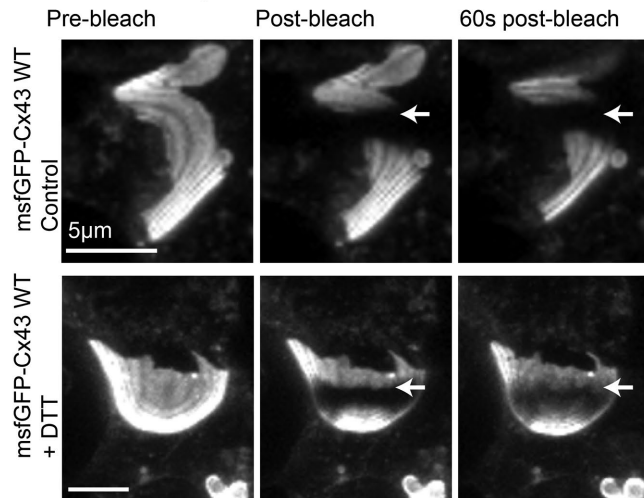
B. Cx43 FRAP at 15s Post-Bleach   C. Cx32 FRAP at 15s
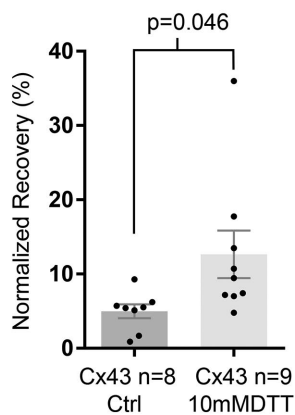
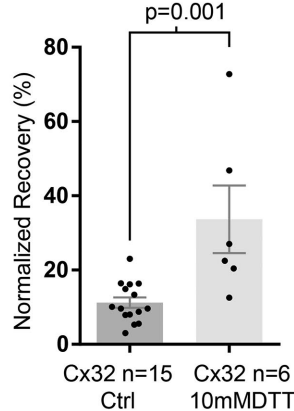**FIGURE 4:** Cellular redox balance controls channel arrangement within GJ plaques. (A) Three-dimensional time-lapse FRAP images of HeLa cells expressing msfGFP-Cx43 (untreated controls, top row), and three-dimensional time-lapse FRAP images of HeLa cells expressing msfGFP-Cx43, treated with 10 mM DTT for 6 h (bottom row). The location of the border of the bleached region of the plaques is indicated by arrows. (B) Percentage recovery of normalized fluorescence into the bleach region at 15 s for msfGFP-Cx43 in HeLa cells using two-dimensional time-lapse FRAP with and without 6-h treatment with 10 mM DTT. (C) Percentage recovery of normalized fluorescence into the bleach region at 15s for msfGFP-Cx32 with and without 6-h treatment with 10 mM DTT. Data for Cx43 and Cx32 are compared separately because there was a significant difference between sfGFP-Cx43 and sfGFP-Cx32 GJ length (Cx32 17.68 ± 2.926 μm vs. Cx43 11.85 ± 0.9938 μm, $p = 0.0375$). Data for untreated controls are sourced from previous figures of this report. Groups in B and C compared by Student's t test (two-tailed).

for future research, which will be facilitated by the basic principles established in this report.

Our results will be important for understanding microstructure of tissues where Cx32 and Cx43 are expressed (e.g., skin, vasculature, heart, liver, kidney, and brain). Recent reports indicate that phosphorylation modifications and connexin binding interactions are localized to subregions of gap junction plaques with both light and electron microscopy (Toyofuku *et al.*, 2001; Sorgen *et al.*, 2004; Gilleron *et al.*, 2008; Cone *et al.*, 2014; Dunn and Lampe, 2014; Solan and Lampe, 2014; Norris *et al.*, 2017). However, if gap junction

plaques are fluidly arranged as they are for Cx26, Cx30, and Cx36, and, as we show in this report for Cx32cyslCT and Cx43cyslCT (and Cx43 and Cx32 under reducing conditions in Hela cells), then such organization would not be possible since phosphorylation-modified GJ channels would disperse throughout the GJ plaque. The ability to experimentally alter the stability of the nexus profoundly through selective mutation of cysteine residues that we demonstrated in this report—without eliminating other residues critical for protein-protein interactions and channel function—will be essential to test how nexus structure affects tissue function in intact animal models. The new way to control GJ plaque organization (cysteine mutagenesis) with fluorescent protein-tagged and untagged connexins that we describe in this report will be valuable for studies on channel *and* non-channel-mediated effects of GJ plaques. Given the location of the cysteine residues within the CT of connexins, the findings we report here should be carefully considered in planning and evaluation of connexin tagging approaches and in validation of results from studies on the GJ nexus.

MATERIALS AND METHODS
Plasmids and subcloning

Fluorescent protein tag location and connexin mutants used in this study are illustrated in Supplemental Figure S1 for clarity; see the Supplemental Material for details on mutagenesis, subcloning strategies, and primer sequences. Connexins with amino-terminal tags form gap junctions (plaques) but do not form functional gap junction channels, while connexins tagged with a carboxy-terminal tags form functional GJ channels but with markedly altered channel gating and interactions with binding partners (Bukauskas *et al.*, 2000; Hunter *et al.*, 2003, 2005). Therefore most of the gap junctions we examined in this study are channel nonfunctional, but it is important to note that we validate the main finding of the study in Figure 2, D–F, by comparing mobility of untagged connexins Cx43 and Cx43cyslCT, which do form functional channels. To achieve this, we used channel-functional Cx43t258-msfGFP expressed in adjacent cells as a proxy for the mobility of the untagged, full-length Cx43 that makes up the other half of the gap junction (Figure 2, E and F, and Supplemental Figures S2 and S4B). The msfGFP-Cx43, Cx43K258stop-msfGFP, sfGFP-Cx26, sfGFP-Cx43K258stop, and EBFP2-Cx30 plasmids were described previously (Stout *et al.*, 2015). Untagged Cx43 and Cx43cyslCT expression was achieved by transfection of the following plasmids: pLv-eEF1α-Cx43_CMV-mCherry, and pLv-eEF1α-Cx43cyslCT_CMV-mCherry, which were produced by the plasmid construction service of VectorBuilder (Cyagen Biosciences). sfGFP-Cx43cyslCT and msfGFP-Cx32cyslCT were produced by mutagenesis and/or gene synthesis by the plasmid construction service of GenScript. sfGFP-Cx43t262, sfGFP-Cx43t268, and sfGFP-Cx43t273 were produced by using PCR amplification and subcloning with primers designed to insert a stop codon and truncate the Cx43 encoding sequence at the specified amino acid (detailed description in the Supplemental Material).

The sfGFP-Cx43d20AA is rat Cx43 with 20 amino acids resected (residues 241–260). The untagged Cx43d20AA (a.k.a. Cx43D250) sequence was a kind gift from Steven Taffet (SUNY Upstate Medical University, Syracuse, NY) and Mario Delmar (New York University School of Medicine, New York, NY) (Homma *et al.*, 1998). The Cx43 encoding sequence with the sectional deletion was inserted in-frame after superfolderGFP as described previously for full-length sfGFP-Cx43 (Stout *et al.*, 2015). The sfGFP-Cx26CT43 plasmid contains the full-length rat Cx26 sequence with sequences encoding an amino-terminal sfGFP-tag linked in-frame to the start of Cx26 by the same eight-amino-acid linker as the control sfGFP-Cx26 and with

the sequence for rat Cx43 CT amino acid section from Cx43 residue K241 through S272 fused by a linker between the CT of Cx26 and the section of the Cx43 CT. Resulting plasmids were verified by sequencing. The cysteine residues in the cytoplasmic carboxy termini of Cx43 and Cx32 are conserved in mice, rats, and humans. We used plasmids to overexpress connexins from rats and humans (Cx43 and Cx32, respectively) in human and mouse cells (HeLa and N2A cells, respectively) to show that the effect of cytoplasmic cysteine residues on GJ plaque stability is a conserved characteristic of the connexin that makes up the GJ, independent of species origin and cell type in which they are expressed.

Cell culture and transfection

A transfection and multi-color fluorescent protein expression schematic is shown in Supplemental Figures S1 and S2 for clarity and described in additional detail in the Supplemental Material. Neuro2a (N2A, ATCC CCL-131) and HeLa cells were maintained in DMEM (glucose 4.5 g/l) supplemented with 10% fetal bovine serum (FBS) and 1% penicillin/streptomycin. For FRAP experiments N2A and HeLa cells were plated into eight-well imaging chambers, and each well was transfected with 0.5 µg of each plasmid to drive expression of connexin-fluorescent protein fusions 24–72 h prior to imaging. Optifect (Life Technologies) was used according to the manufacturer's instructions. Optimem medium was replaced with the standard growth media for HeLa and N2A cells 6–16 h after transfection. Cells were incubated in growth media >4 h after transfection and then transferred to buffered imaging media consisting of DMEM (without phenol-red) supplemented with 10% FBS, 25 mM HEPES, and 2 mM glutamine for image acquisition. HeLa and N2A cells were never cultured together for any experiments in this work. All data presented in the main figures are from HeLa cells with the exception of Figures 2D and 3C, for which N2A cells were used. Cysteine residues in the carboxy terminus of sfGFP-Cx43 and sfGFP-Cx32 as well as untagged Cx43 control plaque stability in N2A cells (Supplemental Figure S4, A–C). The significant fluidizing effect of DTT on Cx43 GJ plaque stability was not observed, although a trend toward increased fluidity was present (Supplemental Figure S4D).

Electrophysiology

Dual whole-cell voltage clamp with voltage ramps in one cell of transfected pairs of N2A cells expressing untagged Cx43cyslCT was performed as previously described (del Corsso et al., 2006) and as detailed in the Supplemental Material.

Two-dimensional time-lapse FRAP

Two-dimensional time-lapse imaging was conducted as described previously (Stout et al., 2015; Stout and Spray, 2016). Cells were maintained at 37°C on the stage of a Zeiss LSM 510 Live with Duo module and imaged with a 63× NA = 1.4 oil immersion objective. The detector consists of dual 512-pixel linear arrays of charge-coupled device camera–type pixels with a slit pinhole that was set to a width of 14 µm for FRAP experiments. Zen 2009 was used to control the confocal microscope and acquire images. GJs aligned in a nearly perpendicular plane with respect to the growth substrate were chosen for two-dimensional time-lapse FRAP. A 10-pixel (2-µm-wide) stripe bleach region was set to bleach a horizontal stripe across each GJ plaque. Bleach settings were 100% laser transmission at a scan speed of 5 with three bleach iterations. Lower bleach laser power and single bleach iterations were tested to evaluate FRAP under conditions of greatly reduced photobleaching as shown in Supplemental Figure S3.

Three-dimesional time-lapse FRAP

Cells were maintained at 37°C on the stage of a Zeiss LSM 510 Live with Duo setup as described above for two-dimensional time-lapse FRAP. GJs aligned in a parallel plane with respect to the growth substrate were used for three-dimensional time-lapse FRAP. The center focal plane of an 11-image Z-stack was set at the z-plane level of the GJ plaque to be tested. The Z-stack step size was set to 0.5 µm. Time interval was set to 3 s. A 10-pixel (2-µm-wide) stripe bleach region was set to bleach a horizontal stripe across each GJ plaque. Bleach settings were 100% laser transmission at a scan speed of 5 with three bleach iterations. Images are cropped and scaled, with the same scaling settings applied to images within each time series but differing slightly between experiments. Three-dimensional reconstructions of the resulting time-lapse FRAP images were performed in Zen 2 software with the maximum reconstruction function. Results from three-dimensional time-lapse FRAP were consistent with the standard two-dimensional time-lapse FRAP experimentation for all of this study, but since the photobleaching event eliminates a different amount of the fluorescent pool available for recovery and the distribution of bleached protein is markedly different than that created in two-dimensional FRAP, the standard two-dimensional time-lapse FRAP was used for quantification while three-dimensional-reconstructed images from three-dimensional FRAP experiments are shown at selected time points that best reveal the additional information provided by three-dimensional FRAP experimentation (e.g., that stability characteristics are consistent from the center to the edge of the GJ plaque structure).

Tagged::untagged FRAP

For FRAP to assess mobility of connexins without a covalent fluorescent protein tag—and as functional GJ channels—we applied FRAP analysis to a connexin isoform to be tested (Cx43 or Cx43cyslCT) bound as a hemichannel to a hemichannel formed of a connexin with established mobility (Cx43t258-msfGFP) as described previously (Stout et al., 2015). Cells were transfected separately, washed twice, and then replated into iBidi eight-well imaging dishes. Fluorescence was used to identify heterotypically tagged GJ plaques, and FRAP experiments were performed in a similar manner as elsewhere in this study. See Supplemental Figure S2 and the Supplemental Material for explanation.

FRAP data analysis

FRAP analysis was performed as previously described (Stout et al., 2015; Stout and Spray, 2016) using ImageJ software (Schneider et al., 2012) (FIJI package [Schindelin et al., 2012]). FRAP experiments were excluded from analysis in cases where the GJ plaque moved outside of the regions of interest (ROIs) used to extract fluorescence data before the 15-s postbleach time point since monitoring whole plaque movement was not the goal of these experiments. We chose the 15-s postbleach time point as the best to balance the need to allow time for potential fluorescence recovery while minimizing confounding phenomena that are particularly problematic for FRAP experimentation on GJ plaques such as movement/drift of the whole GJ plaque within the cell and differences in the pool of fluorescent protein available for recovery (the effects of which are minimized at earlier time points). The ROI tool of ImageJ was used to extract average fluorescence within three ROIs: 1) the bleach region, 2) for the entire GJ plaque to be bleached (fluorescence pool available for recovery [Fp]), and 3) a portion of the background in a location with no GFP expression. Background was subtracted and the percentage recovery within the bleach region ROI was scaled by a correction factor determined by the Fp. The correction factor

corrects for loss of fluorescent pool available for recovery during photobleach and for acquisition-bleach of the pool of fluorescent protein within the confocal imaging plane. The resulting fractional recovery was transformed to percentage recovery and then normalized to 100% prebleach and 0% for the initial postbleach time point to normalize for incomplete bleaching within the bleach ROI as previously described (Snapp and Lajoie, 2011); see the Supplemental Material. The scaled and normalized data points at 15 s after the bleach time point were used in comparison of percentage recovery at 15 s. Statistical comparisons of percentage recovery at selected time points were performed as described in the figure legends for the graphs for each comparison using Graphpad Prism 7 software.

REFERENCES
Ambrosi C, Ren C, Spagnol G, Cavin G, Cone A, Grintsevich EE, Sosinsky GE, Sorgen PL (2016). Connexin43 forms supramolecular complexes through non-overlapping binding sites for drebrin, tubulin, and ZO-1. PLoS One 11, e0157073.

Baker SM, Buckheit RW 3rd, Falk MM (2010). Green-to-red photoconvertible fluorescent proteins: tracking cell and protein dynamics on standard wide-field mercury arc-based microscopes. BMC Cell Biol 11, 15.

Bejarano E, Yuste A, Patel B, Stout RF Jr, Spray DC, Cuervo AM (2014). Connexins modulate autophagosome biogenesis. Nat Cell Biol 16, 401–414.

Bukauskas FF, Jordan K, Bukauskiene A, Bennett MV, Lampe PD, Laird DW, Verselis VK (2000). Clustering of connexin 43-enhanced green fluorescent protein gap junction channels and functional coupling in living cells. Proc Natl Acad Sci USA 97, 2556–2561.

Cina C, Maass K, Theis M, Willecke K, Bechberger JF, Naus CC (2009). Involvement of the cytoplasmic C-terminal domain of connexin43 in neuronal migration. J Neurosci 29, 2009–2021.

Cone AC, Cavin G, Ambrosi C, Hakozaki H, Wu-Zhang AX, Kunkel MT, Newton AC, Sosinsky GE (2014). Protein kinase Cdelta-mediated phosphorylation of Connexin43 gap junction channels causes movement within gap junctions followed by vesicle internalization and protein degradation. J Biol Chem 289, 8781–8798.

Dahl G, Werner R, Levine E, Rabadan-Diehl C (1992). Mutational analysis of gap junction formation. Biophys J 62, 172–180; discussion 180–182.

Del Corsso C, Srinivas M, Urban-Maldonado M, Moreno AP, Fort AG, Fishman GI, Spray DC (2006). Transfection of mammalian cells with connexins and measurement of voltage sensitivity of their gap junctions. Nat Protoc 1, 1799–1809.

Duffy HS, Delmar M, Spray DC (2002). Formation of the gap junction nexus: binding partners for connexins. J Physiol-Paris 96, 243–249.

Dukic AR, Haugen LH, Pidoux G, Leithe E, Bakke O, Tasken K (2017). A protein kinase A-ezrin complex regulates connexin 43 gap junction communication in liver epithelial cells. Cell Signal 32, 1–11.

Dunn CA, Lampe PD (2014). Injury-triggered Akt phosphorylation of Cx43: a ZO-1-driven molecular switch that regulates gap junction size. J Cell Sci 127, 455–464.

Falk MM, Baker SM, Gumpert AM, Segretain D, Buckheit RW 3rd (2009). Gap junction turnover is achieved by the internalization of small endocytic double-membrane vesicles. Mol Biol Cell 20, 3342–3352.

Foote CI, Zhou L, Zhu X, Nicholson BJ (1998). The pattern of disulfide linkages in the extracellular loop regions of connexin 32 suggests a model for the docking interface of gap junctions. J Cell Biol 140, 1187–1197.

Gago-Fuentes R, Bechberger JF, Varela-Eirin M, Varela-Vazquez A, Acea B, Fonseca E, Naus CC, Mayan MD (2016). The C-terminal domain of connexin43 modulates cartilage structure via chondrocyte phenotypic changes. Oncotarget 7, 73055–73067.

Gaietta G, Deerinck TJ, Adams SR, Bouwer J, Tour O, Laird DW, Sosinsky GE, Tsien RY, Ellisman MH (2002). Multicolor and electron microscopic imaging of connexin trafficking. Science 296, 503–507.

Gellhaus A, Dong X, Propson S, Maass K, Klein-Hitpass L, Kibschull M, Traub O, Willecke K, Perbal B, Lye SJ, Winterhager E (2004). Connexin43 interacts with NOV: a possible mechanism for negative regulation of cell growth in choriocarcinoma cells. J Biol Chem 279, 36931–36942.

Gilleron J, Fiorini C, Carette D, Avondet C, Falk MM, Segretain D, Pointis G (2008). Molecular reorganization of Cx43, Zo-1 and Src complexes during the endocytosis of gap junction plaques in response to a non-genomic carcinogen. J Cell Sci 121, 4069–4078.

Gong XQ, Shao Q, Lounsbury CS, Bai D, Laird DW (2006). Functional characterization of a GJA1 frameshift mutation causing oculodentodigital dysplasia and palmoplantar keratoderma. J Biol Chem 281, 31801–31811.

Hammond MA, Berman AG, Pacheco-Costa R, Davis HM, Plotkin LI, Wallace JM (2016). Removing or truncating connexin 43 in murine osteocytes alters cortical geometry, nanoscale morphology, and tissue mechanics in the tibia. Bone 88, 85–91.

Homma N, Alvarado JL, Coombs W, Stergiopoulos K, Taffet SM, Lau AF, Delmar M (1998). A particle-receptor model for the insulin-induced closure of connexin43 channels. Circ Res 83, 27–32.

Hunter AW, Barker RJ, Zhu C, Gourdie RG (2005). Zonula occludens-1 alters connexin43 gap junction size and organization by influencing channel accretion. Mol Biol Cell 16, 5686–5698.

Hunter AW, Jourdan J, Gourdie RG (2003). Fusion of GFP to the carboxyl terminus of connexin43 increases gap junction size in HeLa cells. Cell Commun Adhes 10, 211–214.

Katoch P, Mitra S, Ray A, Kelsey L, Roberts BJ, Wahl JK 3rd, Johnson KR, Mehta PP (2015). The carboxyl tail of connexin32 regulates gap junction assembly in human prostate and pancreatic cancer cells. J Biol Chem 290, 4647–4662.

Kelly JJ, Simek J, Laird DW (2015). Mechanisms linking connexin mutations to human diseases. Cell Tissue Res 360, 701–721.

Kozoriz MG, Bechberger JF, Bechberger GR, Suen MW, Moreno AP, Maass K, Willecke K, Naus CC (2010). The connexin43 C-terminal region mediates neuroprotection during stroke. J Neuropathol Exp Neurol 69, 196–206.

Lauf U, Giepmans BN, Lopez P, Braconnot S, Chen SC, Falk MM (2002). Dynamic trafficking and delivery of connexons to the plasma membrane and accretion to gap junctions in living cells. Proc Natl Acad Sci USA 99, 10446–10451.

Maass K, Chase SE, Lin X, Delmar M (2009). Cx43 CT domain influences infarct size and susceptibility to ventricular tachyarrhythmias in acute myocardial infarction. Cardiovasc Res 84, 361–367.

Maass K, Ghanem A, Kim JS, Saathoff M, Urschel S, Kirfel G, Grummer R, Kretz M, Lewalter T, Tiemann K, et al. (2004). Defective epidermal barrier in neonatal mice lacking the C-terminal region of connexin43. Mol Biol Cell 15, 4597–4608.

Maass K, Shibayama J, Chase SE, Willecke K, Delmar M (2007). C-terminal truncation of connexin43 changes number, size, and localization of cardiac gap junction plaques. Circ Res 101, 1283–1291.

Meyer DJ, Yancey SB, Revel JP (1981). Intercellular communication in normal and regenerating rat liver: a quantitative analysis. J Cell Biol 91, 505–523.

Norris RP, Baena V, Terasaki M (2017). Localization of phosphorylated connexin 43 by serial section immunogold electron microscopy. J Cell Sci 130, 1333–1340.

Orthmann-Murphy JL, Freidin M, Fischer E, Scherer SS, Abrams CK (2007). Two distinct heterotypic channels mediate gap junction coupling between astrocyte and oligodendrocyte connexins. J Neurosci 27, 13949–13957.

Page E, Karrison T, Upshaw-Earley J (1983). Freeze-fractured cardiac gap junctions: structural analysis by three methods. Am J Physiol 244, H525–H539.

Pidoux G, Gerbaud P, Dompierre J, Lygren B, Solstad T, Evain-Brion D, Tasken K (2014). A PKA-ezrin-Cx43 signaling complex controls gap junction communication and thereby trophoblast cell fusion. J Cell Sci 127, 4172–4185.

Pizzuti A, Flex E, Mingarelli R, Salpietro C, Zelante L, Dallapiccola B (2004). A homozygous GJA1 gene mutation causes a Hallermann-Streiff/ODDD spectrum phenotype. Hum Mutat 23, 286.

Rash JE, Yasumura T, Davidson KG, Furman CS, Dudek FE, Nagy JI (2001). Identification of cells expressing Cx43, Cx30, Cx26, Cx32 and Cx36 in gap junctions of rat brain and spinal cord. Cell Commun Adhes 8, 315–320.

Retamal MA, Schalper KA, Shoji KF, Bennett MV, Saez JC (2007). Opening of connexin 43 hemichannels is increased by lowering intracellular redox potential. Proc Natl Acad Sci USA 104, 8322–8327.

Schindelin J, Arganda-Carreras I, Frise E, Kaynig V, Longair M, Pietzsch T, Preibisch S, Rueden C, Saalfeld S, Schmid B, et al. (2012). Fiji: an open-source platform for biological-image analysis. Nat Methods 9, 676–682.

Schneider CA, Rasband WS, Eliceiri KW (2012). NIH Image to ImageJ: 25 years of image analysis. Nat Methods 9, 671–675.

Snapp EL, Lajoie P (2011). Photobleaching regions of living cells to monitor membrane traffic. Cold Spring Harb Protoc 2011, 1366–1367.

Solan JL, Lampe PD (2014). Specific Cx43 phosphorylation events regulate gap junction turnover in vivo. FEBS Lett 588, 1423–1429.

Sorgen PL, Duffy HS, Sahoo P, Coombs W, Delmar M, Spray DC (2004). Structural changes in the carboxyl terminus of the gap junction protein connexin43 indicates signaling between binding domains for c-Src and zonula occludens-1. J Biol Chem 279, 54695–54701.

Sosinsky GE, Gaietta GM, Hand G, Deerinck TJ, Han A, Mackey M, Adams SR, Bouwer J, Tsien RY, Ellisman MH (2003). Tetracysteine genetic tags complexed with biarsenical ligands as a tool for investigating gap junction structure and dynamics. Cell Commun Adhes 10, 181–186.

Stout RF Jr, Snapp EL, Spray DC (2015). Connexin type and fluorescent protein fusion tag determine structural stability of gap junction plaques. J Biol Chem 290, 23497–23514.

Stout RF, Spray DC (2016). FRAP for the study of gap junction nexus macromolecular organization. In Gap Junction Channels and Hemichannels, ed. D Bai and JC Saez, Boca Raton, FL: CRC Press.

Toyofuku T, Akamatsu Y, Zhang H, Kuzuya T, Tada M, Hori M (2001). c-Src regulates the interaction between connexin-43 and ZO-1 in cardiac myocytes. J Biol Chem 276, 1780–1788.

Wang HY, Lin YP, Mitchell CK, Ram S, O'Brien J (2015). Two-color fluorescent analysis of connexin 36 turnover: relationship to functional plasticity. J Cell Sci 128, 3888–3897.

Waxse B, Sengupta P, Hesketh GG, Lippincott-Schwartz J, Buss F (2017). Myosin VI facilitates connexin 43 gap junction accretion. J Cell Sci 130, 827–840.

Wayakanon P, Bhattacharjee R, Nakahama K, Morita I (2012). The role of the Cx43 C-terminus in GJ plaque formation and internalization. Biochem Biophys Res Commun 420, 456–461.